Chapter 5

Bell-mouth integrated SAH for high flow rates

Previous investigations have mainly focused on enhancing the thermal performance of a natural convection solar air heaters (SAH) at the expense of hydraulic performance by incorporating protruded surfaces and, thereby compromising on air mass flow rate significantly due to considerable pressure drop. Low mass flow rate of SAH makes it unsuitable for wide applications. In this chapter the concept of BM in SCPP presented in the previous chapter has been considered for buoyancy-driven SAH. In a first, design investigations using experimentally validated numerical model of SAH is reported that enhances flow rate by more than 100% in comparison to conventional flat plate SAH design. Integration of bell-shaped designs at the inlet of SAH adds to the ram-air effect that converts dynamic pressure into static pressure thereby manifesting into an excellent enhancement of air flow rate as well as in heat transfer associated with less hydraulic losses. The high-flow SAH was further investigated for building application using unsteady first-law of thermodynamic equation and it was observed to be 33% efficient over conventional design. An independent correlation for Nusselt number variation with Rayleigh numbers and bell-mouth ratio of the form $Nu \sim (Racos\theta)^m\,(h/R)^n$ has been developed and found to be in good agreement with the data.

5.1 Introduction

Naturally driven flat plate solar air heaters (SAH) are simple device that utilize solar energy to heat the fluid at ambient condition. The heated air is then utilized in wide applications in the areas such as space heating, drying of agricultural products such as fruits, vegetables and seeds etc. to extend their self-life [121, 131]. Since the availability of solar energy is sporadic, these applications need high flow of heated air to quicken the heating processes. The most common design of natural convection SAH consists of an uniform rectangular cross-sectional duct throughout its length with a glass cover on the top. The incident radiation is absorbed by a collector plate at the bottom the duct. Figure 5.1 shows the conventional design of a solar dryer integrated with flat plate natural convection SAH. One major challenge that scientific communities have mainly focused their investigations are on the design aspect that enhances the heat transfer efficiency in terms of air temperature rise [5, 68, 119, 53]. Heat transfer efficiency is generally measured in terms of energy gain by the cold air while it passes over the heated absorber plate inside the duct [5, 68, 119, 48, 117]. Mathematically, the energy gain is represented as $\dot{m}C_P\Delta T$ where $\dot{m}$ is the mass flow rate of heated air, ΔT is the rise in air temperature and C_P is the specific heat at constant pressure. As depicted in Fig. 5.1, aluminum foil matrix and corrugated aluminum air duct (U-shape) has been used to increase ΔT. With such arrangements, though thermal performance increases in terms temperature gain, however, this gain comes at the expense of hydraulic performance i.e. significant drop in mass flow rate $\dot{m}$. Interestingly, most of the previous investigations have focused on ΔT gain while designing the naturally driven SAH. Considering the fact that natural convection SAH systems have low driving forces and hence, low flow rates, their effectiveness is limited for a short period of time during the day. Clearly, there is a need to investigate the SAH designs that enhances the mass flow rate. Heated high flow air is the primary requirement for many applications as mentioned above.

Though solar collectors have been in use for decades, their external design has fundamentally remained the same. Table 5.1 shows some recent investigations on enhancing the thermal performance of solar collectors. It is noted that the design of SAH has remained the same across the various applications of SAH, i.e. a rectangular

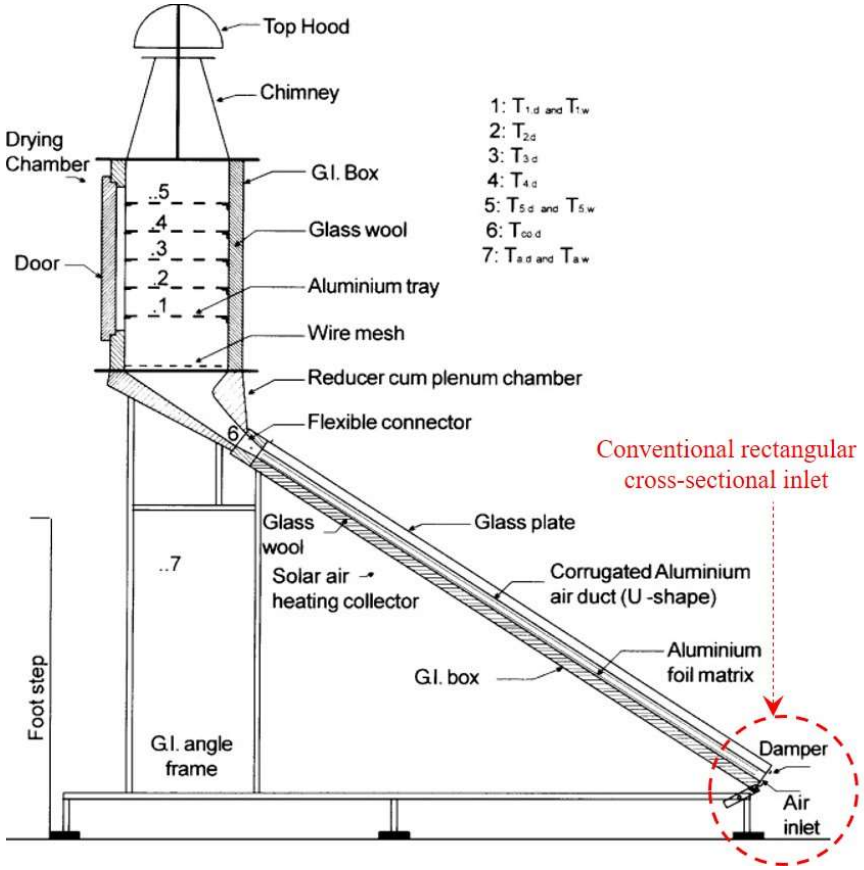

Figure 5.1: Solar dryer integrated with conventional flat plate natural convection solar air heater having rectangular cross-sectional inlet design [121].

inlet and duct design throughout with internal extended surfaces [117].

There are many questions that has not yet been answered in the scientific literature: The query that comes first is that can the air volume flow be increased? Secondly, what optimum design changes can be incorporated in natural convection SAH to increase the air volume flow rates by e.g. double i.e. 100% ? It is natural that high flow would reduce the delivery temperature by some degrees for given energy input. Thirdly, even if the air volume flow rate is increased, will it affect the thermal performance due to drop in delivery air temperature? Or it is still better in comparison to conventional flat plate SAH at high flow rates? In other words, which is better: a low-flow high-temperature SAH design or the design that delivers high-flow low-temperature air? Issues on these lines of thoughts have not yet been addressed in the scientific literature. In this chapter, new bell-mouth designs integrated at SAH inlet and its optimization for enhanced air volume flow rates has been presented, and its performance has been compared to the conventional SAH. The innovative integration of bell-mouth shape designs at inlet and chimney at the outlet of the SAH adds to the ram-air effect that converts dynamic pressure into static pressure, thereby manifesting into an excellent enhancement of air mass flow rate and hence, increase in Nusselt number.

The concept of enhancing air mass flow rates by bell shape designs that adds to the ram-air effect is common in high-performance engines [67, 61], higher discharge efficiency in vertical intakes [109], improved aerodynamic performance of outdoor unit of air conditioner [156, 66] and many other applications. However, the effect of such designs vis-à-vis natural convection solar air heaters have not been documented in the scientific community. Enhanced mass flow rates of SAH would be a boon especially for high altitude regions on earth where air density is low due to low atmospheric pressure. Although there can be many other designs that may enhance mass flow rates, the major focus of this investigation is to keep the original design of SAH intact and explore the designs that can be easily incorporated into the original design without major modifications and cost inputs. We hope that these new designs would assist the scientific community in further developing efficient designs for harnessing solar energy efficiently.

Table 5.1: Literature survey of conventional rectangular shaped cross-sectional inlet of different natural

convection solar air heaters.

Authors	Study	Parameters of SAH and design	Conclusions
[151]	Effect of channel depth on energy gain in natural convection SAH having rectangular inlet was investigated numerically.	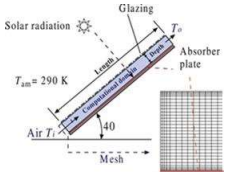 Channel depth	Reducing channel depth substantially increases friction loss, while increasing the depth magnifies heat loss to ambient.
[101]	Experimental analysis on natural convection SAH comprises of top glass and sine-wave absorber in a cross-corrugated SAH with rectangular inlet section.	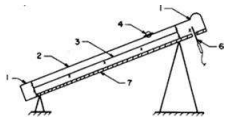 Solar radiation intensity, spacing (i.e. gap between glass and absorber), air temperature and flow rate.	Maximum efficiency near to 0.7 for higher spacing greater than 0.05 m. On the other hand higher temperature was observed for smaller spacing.
[157]	Developed a cost effective natural and forced convection SAH for space heating having rectangular cross-sectional inlet.	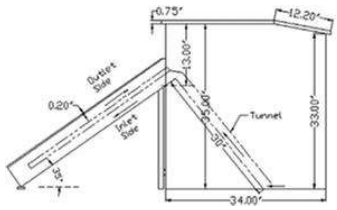 Temperature of absorber, glass, air inlet and outlet, room.	The room temperature was maximum of 45.5 °C and 41.75 °C for forced and natural convection mode, respectively, showed that the room heating was more efficient by forced circulation.
[131]	Solar air dryer for corn drying was numerically studied having conventional rectangular shape inlet.	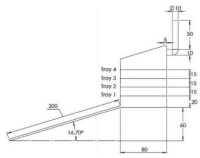 Weather dependence drying performance was analyzed in terms of moisture content.	Presented design of solar air dryer improved the natural circulation rate by diminishing stagnation zones which increase the rate of moisture removal and drying efficiency.
[148]	Experimentally studied the optimum spacing between glass–absorber and absorber–insulation of SAH.	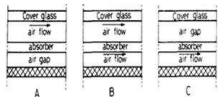 Gap between glass cover and absorber plate, and number of glass covers.	Decreasing the spacing between glass and absorber is more significant for heat transfer. By decreasing the spacing, the heat transfer coefficient between absorber and flow increases.
[9]	Investigated optimum tilt angle of flat natural convection SAH.	 Inclination angle of SAH with horizontal plane.	The best collector performance has been achieved at a collector inclination angle of 50° in terms of maximum Nusselt number and collector efficiency.

[18]	Conducted energy and exergy analysis of natural convection SAH having rectangular cross-sectional inlet.	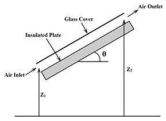 • Number of glass covers for different fins arrangements such as longitudinal fins with rectangular and triangular shape. • Depth and length of the flow channel.	Showed that two glass cover minimize the heat loss more effectively and hence thermal efficiency of the device increases. The thermal performance was more for triangular fins arrangements compared to rectangular fins.
[64]	Experimentally evaluated the thermal performance of a double parallel flow natural convection SAH with rectangular inlet section.	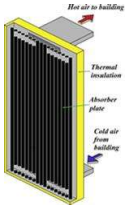 Air flow velocity and temperature gradient between the collector and the building.	Daily values of thermal efficiency lies in the range 0.48 and 0.5 under clear sky, while 0.41 and 0.46 during semi-cloudy days. The percentage error variation between experimental data with the analytical were 307% for temperature and 5% for useful energy produced.
[63]	Determined natural convection heat transfer coefficient in a vertical flat plate with two glass cover was experimentally studied.	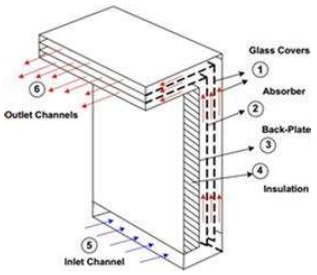 Number of glass covers and multiple vertical channels for flow circulation.	The maximum thermal efficiency was associated with the solar air heater device with three channels among different considered cases.
[115]	Explained thermosyphon solar air heating system.	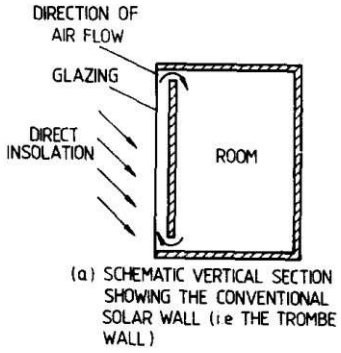 Different circulation loops for room heating such as S-loop, Trombe wall and center-glazed collector.	Fins perpendicular to the air flow movement were reported thermally more efficient than those with inline/along flow. Fins placed perpendicular to the flow was shown substantially better for enhanced thermal performance.

[166]	A zero-energy thermal catalytic-Trombe wall was experimentally reported without auxiliary energy under constraint formaldehyde degradation under exposure of solar radiation.	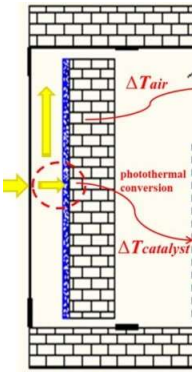 Solar radiation, surrounding temperature, and air layer thickness.	Experimentally showed the total energy saving of 97.4 kW h/ m2. The energy saved for space heating and formaldehyde degradation as 63.4 kW h/m2 and 33 kW h/m2, respectively.
[141]	Numerically investigated thermal performance of convex-concave curved natural convection SAH.	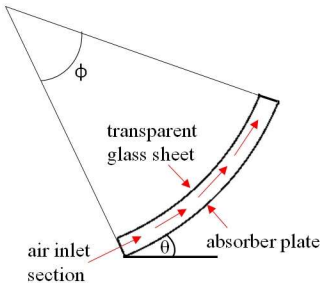 Curvature angle of concave and convex SAH.	The term Nusselt number per unit pressure drop was maximum for convex curvature angle i.e. 7% and 43% higher thermal effectiveness when compared with conventional flat SAH design.

5.2 Designs and the computational model

Figure 5.2(a) shows the inlet design of the SAH and Fig. 5.2(b) shows the enlarged view of the inlet section. The bell-mouth (BM) shape inlet design is a function of circle radius R and height$h$. Effect of different h/R ratio (see Table 5.2) on SAH performance has been investigated. Note that h/R can also be expressed as a function of tube diameter. All the SAH designs considered in this chapter are kept at a fixed constant angle of inclination, = 45° w.r.t. horizontal plane throughout the study. This angle was experimentally observed to be optimum from heat transfer point of view [53]. To augment the effect of bell shape design on SAH performance, a long narrow passage in the form of a chimney (see Fig. 5.2) is also investigated for different design parameters of bell-mouth.

Table 5.2: Range of geometric and operating parameters.

S. No.	Parameters	Values of parameters
1	bell-mouth ratio, 'h/R'	0.3-0.6 for R= 50 mm 0.1-0.3 for R=100 mm
2	Chimney height (fixed)	2000 mm
3	Absorber heat flux (W/m^2)	500, 600, 700, 800, 900, 1000, 1100
4	Air velocity at the air inlet section	Stagnation state
5	SAH inclination w.r.t. horizontal plane (θ)	45° (fixed)

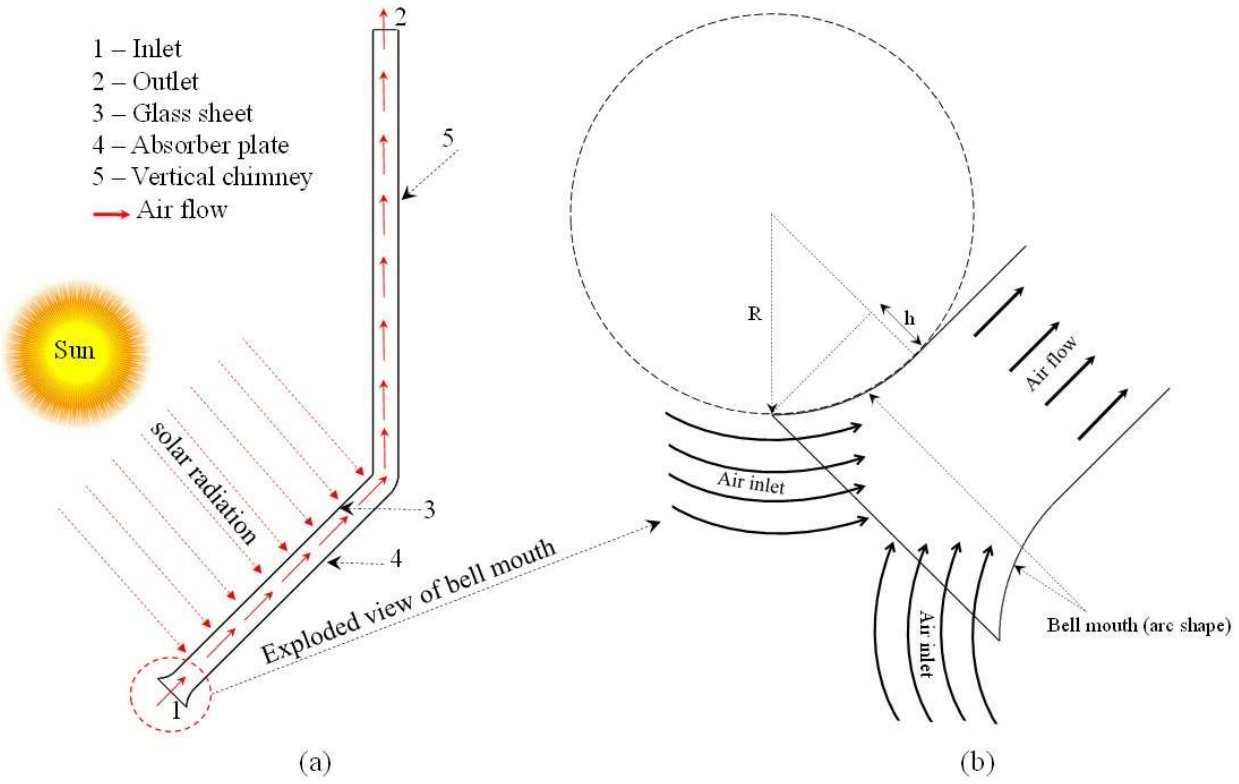

Figure 5.2: (a) Flat plate natural convection SAH integrated with bell-mouth at the SAH inlet and chimney at the SAH exit; (b) Enlarged view of inlet section.

5.2.1 Design details and geometric parameters

The rectangular flow channel (duct) comprises of the top glass surface, absorber plate, air inlet and outlet sections. The two-dimensional SAH model is 1100 mm in length and opening height, H (i.e. the distance between top glass and absorber plate) is 102 mm, which are same as the experimental design of the literature [53]. The conventional SAH is integrated with bell-mouth at the SAH inlet as shown in Fig. 5.2(a) & (b). A vertical chimney of height 2000 mm is attached at the exit of SAH (Fig. 5.2(a) & (b)). The opening thickness at the outlet of chimney is 102 mm to guide the upcoming air flow (Fig. 5.2(a)). The absorber plate has been set to a constant heat flux (q) value in the range of $500 - 1100$ W/m^2. At inlet, the air drawn due to buoyancy effect created by the hot absorber plate. The heated air gradually rises upward in the SAH duct. The basic geometrical and operating parameters are listed in Table 5.2.

5.2.2 Mesh generation and grid independence test

The trias shape unstructured mesh are used to discretize the flow domain. Fine unstructured mesh with multiple boundary layers adjacent to walls are created along the channel to capture the air flow characteristics of the buoyancy driven flow as shown in Fig 5.3. This helps in accurately predicting the flow vortices and friction losses in the boundary layer. The dimensionless wall distance (y^+) has been kept less than unity by sufficiently refining the mesh near the wall. Analysis and modeling has been done using Altair HyperWorks software.The same numerical model reported by [141] has been used in this investigation. The procedure adopted for the grid independence test is identical to the published chapter by the same authors. Interested readers can refer to appendix A of chapter **??**[141] for more details. For brevity, the detailed procedure has not been presented here.

5.2.3 Boundary conditions

The air inlet of SAH was kept as stagnation pressure condition to match surrounding condition. The movement of air through the flow channel occurs due to buoyancy effect when air comes in contact with the hot absorber plate. The above boundary condition is adopted for naturally driven flows where the inlet conditions are

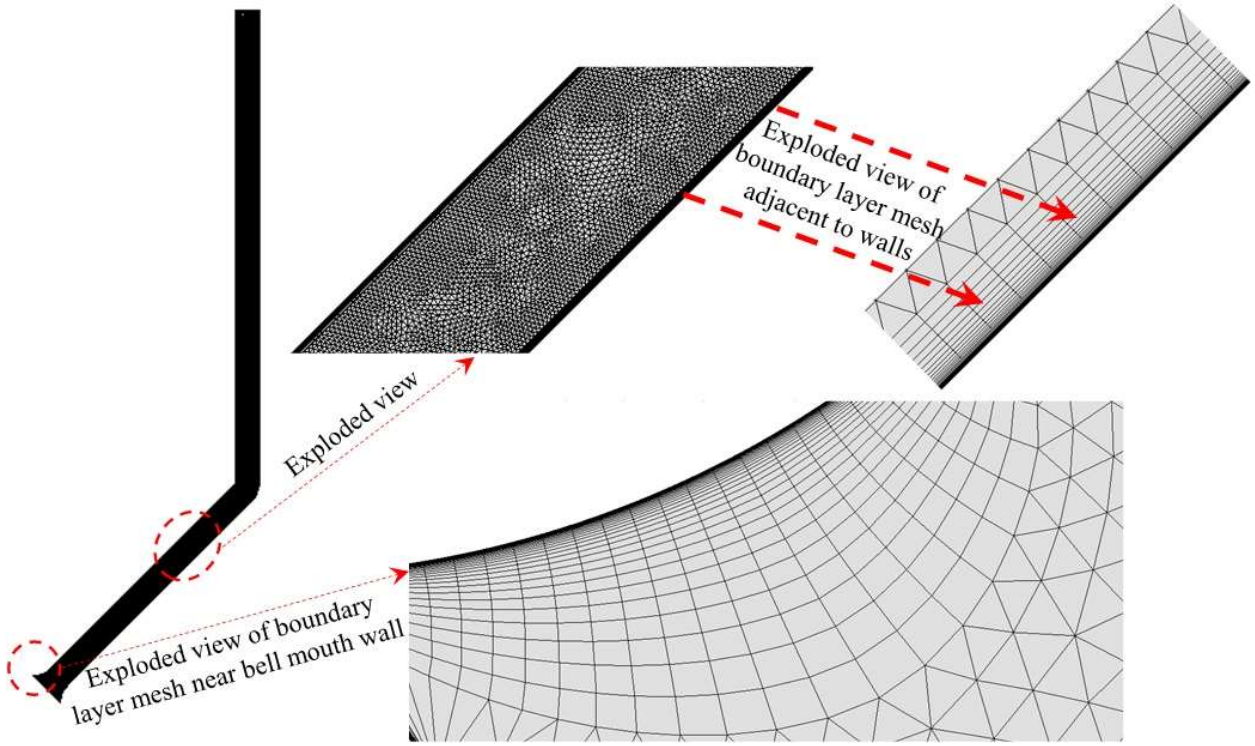

Figure 5.3: Computational mesh domain of the natural convection SAH integrated with bell-mouth and chimney. Boundary layer mesh is shown in the magnified views.

unknown. A constant heat flux condition was assigned to the absorber plate. The outlet condition was assigned at the outlet. The other walls of the SAH were assumed as adiabatic and set to no-slip boundary condition. For the temperature gradient less than 30 °C, the Boussinesq approximation show more accurate results [85, 168]. However, when the temperature difference exceeds 30 °C, a significant deviation from the actual flow field had been observed with Boussinesq solution. Hence, in the present study computational model has been developed treating air as an ideal gas [141]. Air property like density (ρ), thermal conductivity (k), viscosity (μ) and specific heat (C_P) changes with temperature. We have taken care of density change by modeling air as ideal gas which uses ideal gas law to express density as a function of temperature and pressure. However, we have kept other property constant. This is justified in the range of temperature variations of air in solar air heater. For example, value of air Prandtl number ($Pr = \mu C_P/k$) is 0.713 at 300 K while it is 0.684 at 450 K i.e. only 4% change in this range of temperature variation, which is insignificant. Even if variable properties are used, results wouldn't change significantly from what is presently reported in this chapter. The thermo-physical properties of air at the inlet section of SAH has been listed in Table 5.3.

Table 5.3: Air properties at the inlet of SAH at ambient temperature of 300 K.

Properties name	Value
Dynamic viscosity (μ)	1.855 x 10-5 Ns/m^2
Thermal conductivity (k)	0.026 W/m K
Prandtl number (Pr)	0.71
Specific heat (C_P)	1003.62 J/kg K
Density (ρ)	1.184 kg/m^3

5.2.4 Necessary physics models and governing equations

The finite volume method (FVM) is used for discretization of the computational flow domain. The flow domain is exposed to sets of boundary conditions in order to obtain variation in characteristics of the different SAH devices in terms of mass flow rate of air (m), Nusselt number (Nu) and coefficient of pressure (C_P). The dependent variable is the dimensionless Nusselt number (Nu) obtained using Eq. 5.1 [53].

$$Nu = \frac{h_{avg} H}{k_a} \tag{5.1}$$

where h_{avg} is the convection heat transfer coefficient $= \frac{1}{A}\int_A \frac{q_{conv}}{(T_s - T_a)} dA$, where H is the duct height (i.e. gap between top and bottom surface of the SAH duct), h_{avg} is the convective heat transfer coefficient at the hot absorber plate and k_a is the thermal conductivity of air.

The Rayleigh number (Ra) was calculated using basic Eq. 5.2 [68, 119, 53].

$$Ra = \frac{\rho^2 \beta C_P g \Delta T L^3}{\mu k_a} \tag{5.2}$$

where ρ is the air density, β is the volumetric expansion coefficient (K^{-1}), μ is the dynamic viscosity of air (Ns/m^2), $\Delta T = T_s - T_a$(K) where $T_s$is average temperature of absorber surface (K) and T_a is ambient temperature (K), g is the gravitational constant ($m.s^{-2}$), and L is the absorber plate length. The Rayleigh number (Ra) is a dimensionless number directly proportional to the temperature difference between absorber plate surface and surrounding air.

The values of Rayleigh number in the present study was of the order higher than 10^9, which represents turbulent flow, and therefore two-equation realizable K-Epsilon model with two- layer approach was used in this study[110, 116] . The realizable K-Epsilon model is capable to perform well at all dimensionless wall distance (y^+) with full buoyancy effect [140, 141]. Very fine mesh region was generated near walls of the SAH to resolve laminar sub-layer. The dimensionless wall distance near walls has been found less than unity. Two-dimensional computational flow domain was analysed considering air as an ideal gas under steady state flow condition. Many authors have reported natural convection flow analysis using steady state condition [91, 110, 124]. Viscous dissipation term is more pronounced in high speed flows especially, when the viscosity of the fluid is high such as flow of oil in journal bearings. In solar air heater, the air is the fluid medium possess very low density and slowly marches in the flow channel, and hence the term viscous dissipation term has been neglected as the flow is driven due to buoyancy forces. Second order upwind scheme was used to solve governing equations. The results were recorded when changes in parametric variations became negligible with respect to successive iterations. The continuity, momentum and energy equations [141, 124, 116] were solved for two-dimensional computational domain.

Continuity equation

$$\frac{\partial(\rho u)}{\partial x} + \frac{\partial(\rho v)}{\partial y} = 0 \tag{5.3}$$

Momentum equations

$$\frac{\partial(\rho u u)}{\partial x} + \frac{\partial(\rho u v)}{\partial y} = -\frac{\partial p}{\partial x} + \frac{\partial}{\partial x}\left[(\mu + \mu_t)\frac{\partial u}{\partial x}\right] + \frac{\partial}{\partial y}\left[(\mu + \mu_t)\frac{\partial u}{\partial y}\right] - \frac{2}{3}\rho\frac{\partial k}{\partial x} \tag{5.4}$$

$$\frac{\partial(\rho u v)}{\partial x} + \frac{\partial(\rho v v)}{\partial y} = -\frac{\partial p}{\partial y} + \frac{\partial}{\partial x}\left[(\mu + \mu_t)\frac{\partial v}{\partial x}\right] + \frac{\partial}{\partial y}\left[(\mu + \mu_t)\frac{\partial v}{\partial y}\right] - \frac{2}{3}\rho\frac{\partial k}{\partial y} - (\rho - \rho_0)g \tag{5.5}$$

Energy equation

$$\frac{\partial(\rho u T)}{\partial x} + \frac{\partial(\rho v T)}{\partial y} = \frac{\partial}{\partial x}\left[\left(\frac{K}{C_P} + \frac{\mu_t}{Pr_t}\right)\frac{\partial T}{\partial x}\right] + \frac{\partial}{\partial y}\left[\left(\frac{K}{C_P} + \frac{\mu_t}{Pr_t}\right)\frac{\partial T}{\partial y}\right] \tag{5.6}$$

where k is the turbulent kinetic energy, μ_t is the turbulent viscosity and Pr_t is the turbulent Prandtl number which is the ratio of eddy diffusivity for momentum $\left(\varepsilon_M = \frac{\overline{-u'v'}}{\frac{\partial \overline{u}}{\partial y}}\right)$ and heat transfer $\left(\varepsilon_H = \frac{\overline{-v'T'}}{\frac{\partial \overline{T}}{\partial y}}\right)$. The other two turbulent kinetic and dissipation equations are:

$$\nabla \cdot (\rho k \overline{V}) = \nabla \cdot \left[\left(\mu + \frac{\mu_t}{\sigma_k}\right)\nabla k\right] + G_k + G_b - \rho\varepsilon - \gamma_M + S_k \tag{5.7}$$

$$\nabla \cdot (\rho \varepsilon \overline{V}) = \nabla \cdot \left[\left(\mu + \frac{\mu_t}{\sigma_\varepsilon}\right)\nabla \varepsilon\right] + C_{\varepsilon 1}\frac{\varepsilon}{k}(G_k + C_{\varepsilon 3} G_b) - C_{\varepsilon 2}\rho\frac{\varepsilon^2}{k} - R_\varepsilon + S_\varepsilon \tag{5.8}$$

G_k and G_b denotes turbulent production and buoyancy production, respectively.

The values of parameters σ_T , σ_k , and σ_ε are 1.0, 1.0, and 1.2, respectively, whereas turbulence model constants i.e. $C_{\varepsilon 1}$ =1.44, $C_{\varepsilon 2}$ =1.9 and C_μ =0.09, where Pr = 0.9.

The SIMPLE (semi-implicit method for pressure linked equations) algorithm is used to simplify and solve the velocity and pressure fields for the discretized numerical domain. The convergence criteria for energy equation was considered of the order 10^{-4} and 10^{-5} for velocity components.

5.2.4.1 Experimental set-up for validation

The computational model was validated with the experimental and numerical data of the literature [34]. The effect of turbulent natural convection in a large vertical channel with one-sided heated wall was studied. The channel width is 50 m, the height is 8 m and depth is 0.5 m. A two-dimensional model was considered which is dimensionally identical to the experimental set-up [34] having vertical channel of height (H) 8 m and width (L) 0.5 m. One wall of the channel was maintained at constant temperature 423 K with wall emissivity (ε) 0.9. The temperature of air at the inlet section has been taken 293 K. The temperature profile variation across the channel width have been compared with experimental and numerical results [34] as shown in Fig. 5.4. The temperature profile obtained using numerical results of the present study are in good agreement with the experimental and numerical results of the literature [34].

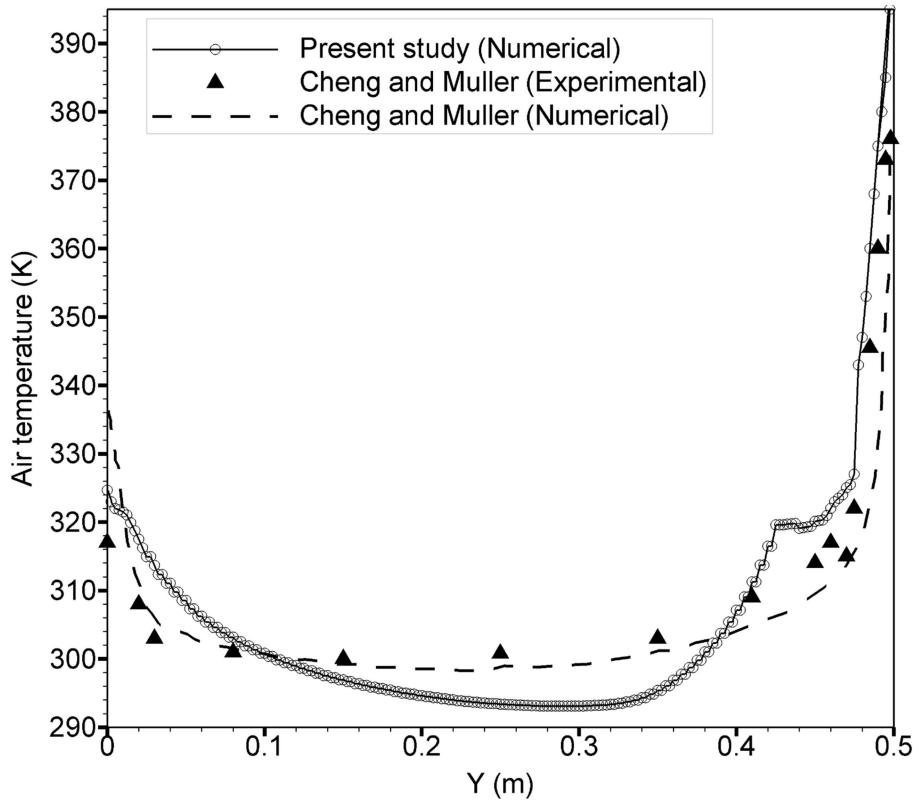

Figure 5.4: Validation of the present numerical model with experimental and numerical results of the literature [34]. The temperature profiles across the channel width at H=7.8 m have been compared.

To care of the radiative and convective losses from the top glass, the top surface is assigned the heat transfer coefficient value $h = 5.7 + 3.8V_\infty$ W/m^2-K [150, 154, 142], where V_∞ is environmental wind velocity, which is assumed as zero for standstill condition.

5.2.5 Pressure coefficient variation

Pressure coefficient variation indicate the dynamic condition of the system and used to study fluid flow. The expression is provided below in Eq. 5.9:

$$C_P = \frac{(P - P_\infty)}{\frac{1}{2}\rho_\infty V_\infty^2} \tag{5.9}$$

where P is the static pressure at the point where C_P is being measured, ρ_∞ is the fluid density of the free stream, P_∞ is the static pressure of free stream, and V_∞ is the velocity of free stream. Total pressure is given as,

$$P_{total} = \frac{1}{2}\rho v^2 + P_{static} \tag{5.10}$$

where ρ is the density of fluid, v is the velocity of fluid, P_{static} is the static pressure at a particular location, and $\frac{1}{2}\rho v^2$ is the dynamic pressure.

In fluid dynamics, the Mach number (M) is a dimensionless quantity, which is the ratio of the flow velocity 'V' to the local speed of sound 'c' (i.e. $M = \frac{V}{C}$). In the present study, the flow velocity is very low at the inlet of SAH, the corresponding value of Mach number always be less than 0.3 ($M < 0.3$). The flow is treated as incompressible throughout the study as the M is less than 0.3. Hence, the above coefficient of pressure formula is valid for our analysis. The zero value of C_P indicates that the pressure is same as that of free stream pressure. The C_p value of one corresponds to stagnation pressure and indicates the stagnation point. The zero and negative values corresponds to cavitation state or low pressure zone, while non-cavitation state for positive values of C_P.

Since the atmospheric air is at the stagnation state (i.e. air velocity is zero), the total pressure at the inlet equals to atmospheric pressure (P_{atm}), which is taken as reference pressure. The dynamic and static pressure balance each other, therefore increase in the flow velocity while air is drawn at the SAH inlet reduces the static pressure and increases the dynamic pressure. This results in negative C_P values near the absorber plate at inlet section of SAH. Clearly, ram-air effect of the bell-mouth design can be investigated by studying the variation of pressure coefficient at the inlet of SAH. To get better insights into the design effects, local variation of flow parameters has also been presented.

5.3 Results and discussions

Effect of two different designs on SAH energy conversion were investigated in the present study: 1. Conventional flat plate SAH integrated with bell-mouth and 2. Conventional flat plate SAH integrated with bell-mouth and chimney (see Fig. 5.2). The objective is to enhance the mass flow rate of heated air of conventional flat natural convective SAH, with insignificant additional hydraulic losses and fabrication cost. The data obtained for various designs are presented in terms of mass flow rate (m), inlet velocity variations, pressure coefficient (C_P) and Nusselt number (Nu) for each case. A significant enhancement in mass flow rate and thermal performance over the conventional flat design has been observed.

5.3.1 Effect of bell-mouth design (Flat + bell-mouth)

It is observed that except for some cases of bell-mouth design, all other designs show enhancement of mass flow rates over the conventional flat plate SAH. The maximum percentage increase in mass flow rate of heated air over conventional SAH was found to be about 18% for bell-mouth ratio, *h/R=0.6, R=50* mm at a constant heat flux of 1100 W/m^2. Change in average velocity at inlet would also reflect in local velocity and pressure coefficient variation. Fig. 5.5 shows the velocity of air at the SAH inlet for different designs of bell-mouth. Measured location of velocities has been marked in the figure as inset. Significant velocity gradient is clearly visible. Lower velocity (near 0 mm) to higher velocities (near 102 mm) is seen due to buoyancy effect. This gradient is stronger in case of bell-mouth design with $h/R = 0.6$ and radius $R = 50$ mm. How it is possible that velocity increases for the same energy input? This has been discussed later.

Figure 5.6 shows the pressure coefficient (C_P) distribution at the inlet section. The shape of bell-mouth with dimension *h/R =0.6, R=50* mm contribute to significant negative C_P values in the range –0.0025 to –0.0235, and hence, the maximum increase in local flow velocity of about 17% has been seen in comparison to

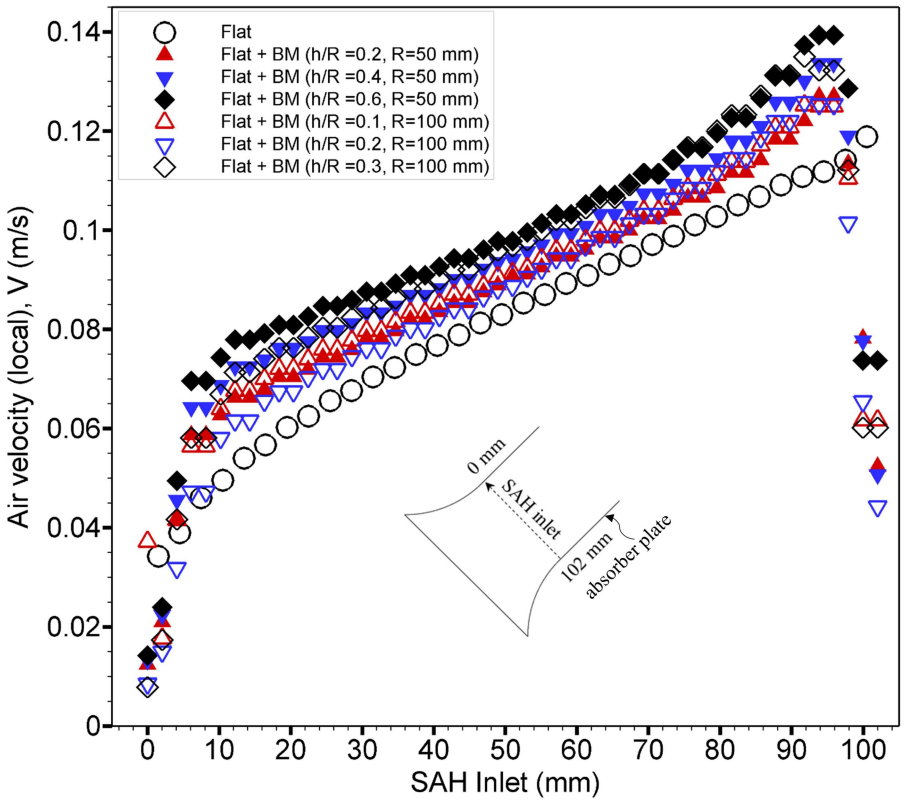

Figure 5.5: Variation of local air flow velocity at the inlet integrated with different shapes of bell-mouth (h/R in the range 0.1-0.6) at absorber heat flux of 1000 W/m^2. Measured location (0 mm -102 mm) has been marked in the inset.

conventional flat SAH design (see Fig. 5.5). The velocity of air increases on account of reduction in pressure coefficient.

Figure 5.7 demonstrates the variation in Nusselt number with Rayleigh number (Ra) for different designs. The characteristic length, L_c i.e heated length was used to calculate Ra. It is noticed that except for the bell-mouth design with $h/R = 0.2$ and $R = 100$ mm, all other designs of bell-mouth perform better in comparison to the conventional design due to enhanced flow rates. It is also interesting to observe that as the magnitude of the Rayleigh number increases, differences in thermal performance also increases. bell-mouth design with ratio $h/R = 0.6$, $R = 50$ mm shows higher Nusselt number values, which indicates enhanced flow inside the duct.

5.3.2 Effect of bell-mouth design with chimney (Flat + bell-mouth + chimney)

The conventional flat plate natural convection SAH has been integrated with the bell-mouth geometry at the inlet of SAH and the vertical chimney at the exit of SAH as shown in Fig. 5.2. The effect of different shape of bell-mouth design with chimney have been investigated and discussed in this sub-section.

Figure 5.8 shows the effect on mass flow rate when the conventional SAH is equipped with various shapes of bell-mouth and chimney. Four different cases are compared: performance of the conventional flat plate, flat plate with various bell-mouth designs (flat + BM), flat plate integrated with a chimney (flat + chimney) and flat plate integrated with chimney and various bell-mouth designs (flat + chimney + BM). Some interesting observations are as follows: (a) without chimney the bell-mouth design with $h/R = 0.6$, R = 50 mm showed better thermal performance than other BM designs (see Fig. 5.7) but when chimney is integrated, the bell design with h/R =0.3, R =100 mm (larger inlet area) show higher mass flow rates, (b) When compared with the flow rates of conventional flat SAH design alone, the combination of flat + BM and flat + BM + Chimney, the maximum enhancement in mass flow rates of about 18% and 111% respectively are observed. One reason for observation (b) above is that as mass flow rates of the SAH increases, an inlet with a larger flow area adapts better with the new flow conditions.

Figure 5.9 shows the pressure coefficient (C_p) distribution at the inlet of SAH with bell-mouth integrated with chimney. Lower the $C_p$value higher would be the flow rate. It is noticed from the figure that conventional

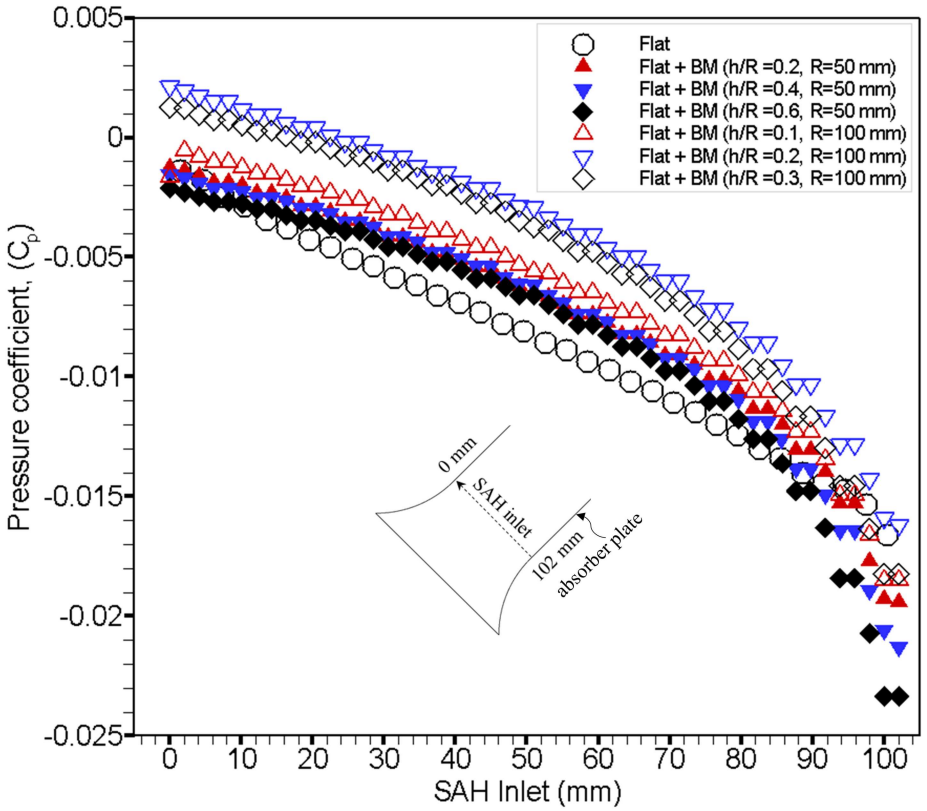

Figure 5.6: Variation of local pressure coefficient (C_P) at the inlet integrated with different shape of bell-mouth (h/R in the range 0.1-0.6) at absorber heat flux of 1000 W/m^2. Measured location (0 mm -102 mm) has been marked in the inset.

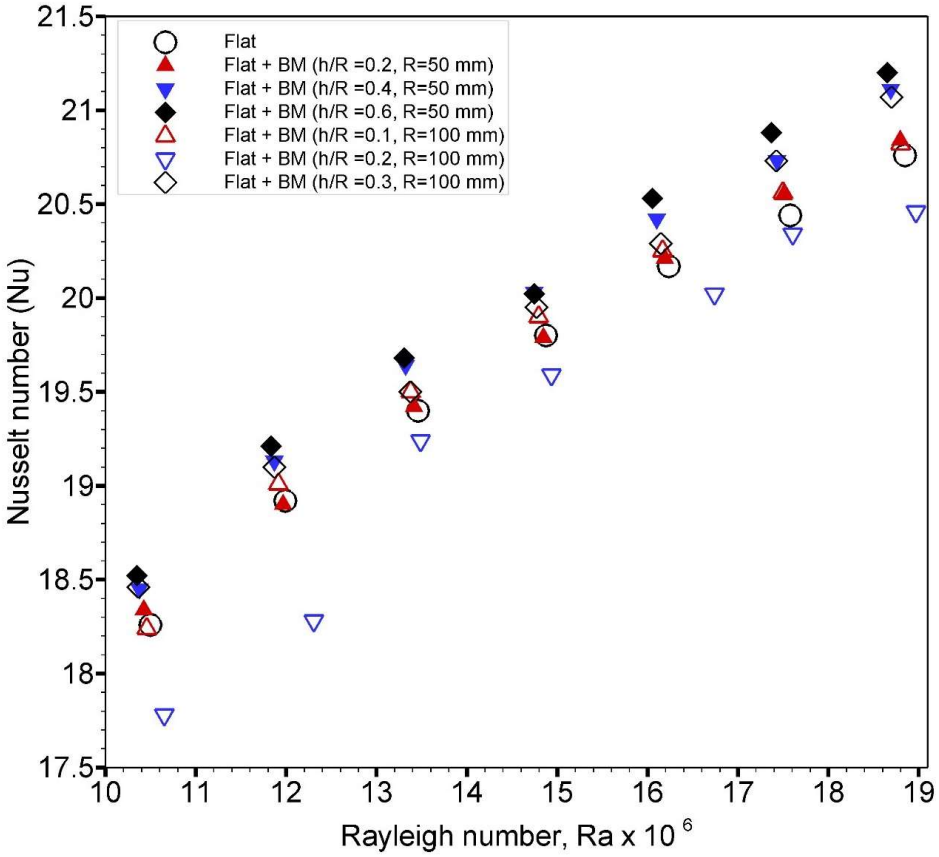

Figure 5.7: Variation of Nusselt number of SAH integrated with different shape of bell-mouth (h/R in the range $0.1 - 0.6$) with Rayleigh number.

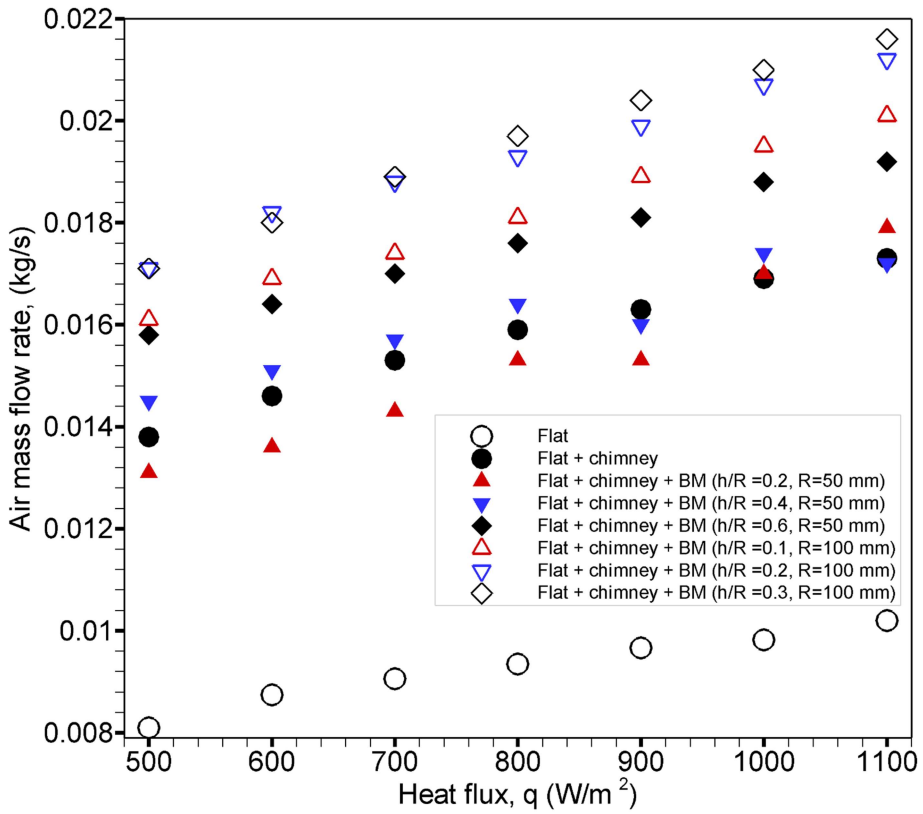

Figure 5.8: Variation of mass flow rate when integrated with different shape of bell-mouth (see legend) with chimney at different solar insolation.

flat plate design has higher C_p than all other designs of bell-mouth. The flat SAH system with only chimney has intermediate C_p values but when integrated with bell-mouth show significant reduction in C_p values. The shape of bell-mouth having dimension $h/R = 0.1, R = 100\,mm$ display C_p values in the range –0.031 to –0.012 and closely followed by bell-mouth design of $h/R = 0.2$, $R = 100$. Maximum drop in C_p with bell-mouth and chimney was 22.12 % lower than conventional flat SAH**.** The effect of changes in local pressure coefficient manifests into corresponding changes in local air velocity at that location as shown in Fig. 5.10. It can be noticed that the conventional flat plate design of SAH show significantly low air velocity for the same driving force. Integration of bell-mouth and chimney enhances dynamic performances considerably.

Figure 5.11 demonstrates the variation of Nusselt number with Rayleigh numbers for different solar insolation. Higher Nusselt number values is observed with the configuration flat + chimney + BM for wider opening of bell-mouth. The maximum percentage increase in Nu was found to be about 9% with bell-mouth ratio$h/R = 0.3$, $R = 100mm$ when compared to conventional flat SAH design. It is to be noted that about ten percent increase in Nu has been achieved without changing the basic design of conventional SAH and without significantly comprising on dynamic performance.

5.3.3 Why flow rate increases with the integration of bell-mouth design at inlet?

It has been observed in the previous sections that integration of bell-mouth designs at the inlet of a conventional natural convection SAH enhances air mass flow rates significantly for a given energy input. This is possible only by two ways: either by increasing the energy input to the system or by reducing the losses from the system. Since the energy flux to the system remains constant, air can speed up only if internal losses are minimized. Internal losses are a function of geometric parameters. Since the basic design of conventional SAH has not been altered, how is it possible to reduce losses?

Figure 5.12(a) shows the schematic representation of flow at the inlet of a conventional flat plate SAH and Fig. 5.12(b) is for a SAH with bell-mouth at the inlet. Flow enters from a large reservoir in both the designs. Air undergoes sudden contraction from section 1-1 to the inlet. This contraction continues till some further distance after the inlet till it reaches at section c-c i.e. vena contracta. To conserve mass, the velocity at vena

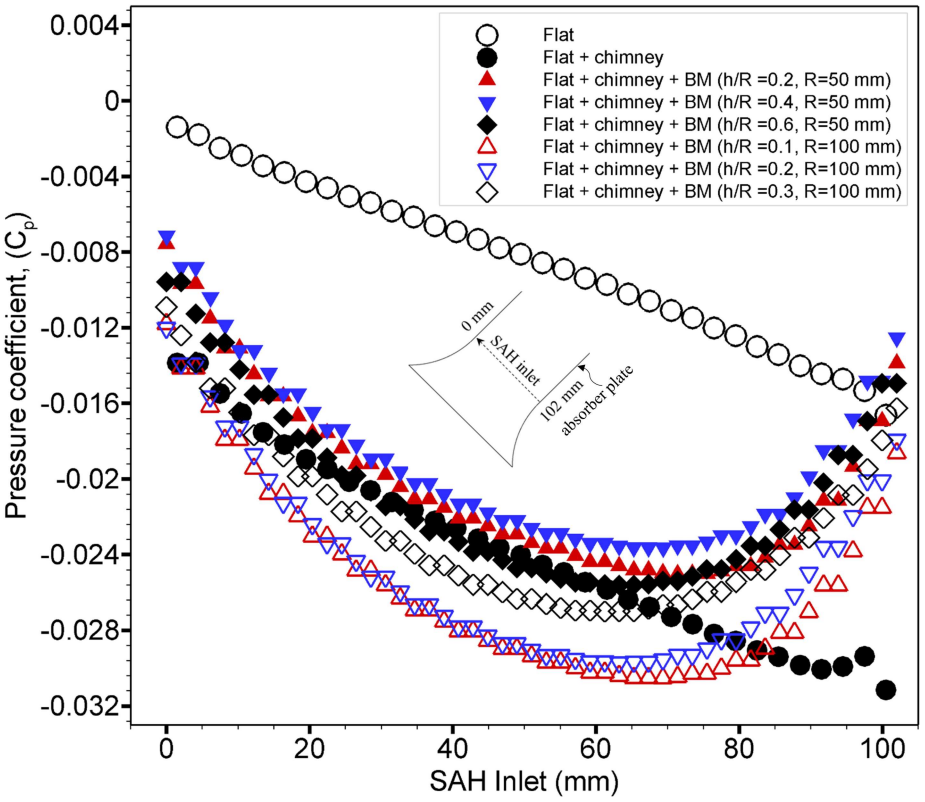

Figure 5.9: Variation of pressure coefficient (C_p) at the inlet of SAH integrated with different shape of bell-mouth with chimney, at absorber heat flux of 1000 W/m^2.

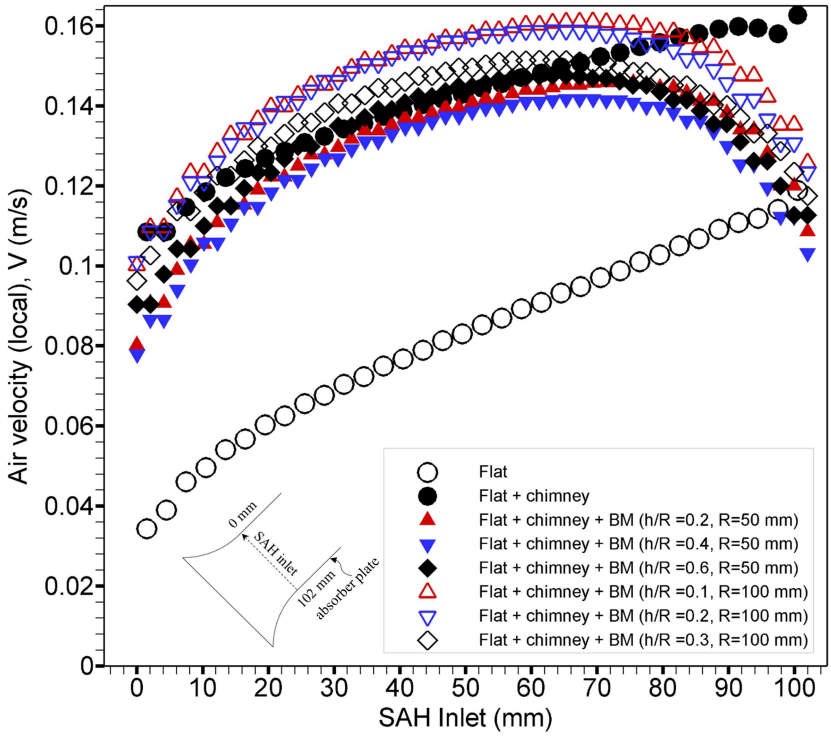

Figure 5.10: Variation of local air flow velocity at the inlet of SAH integrated with different shape of bell-mouth with chimney at absorber heat flux of 1000 W/m^2.

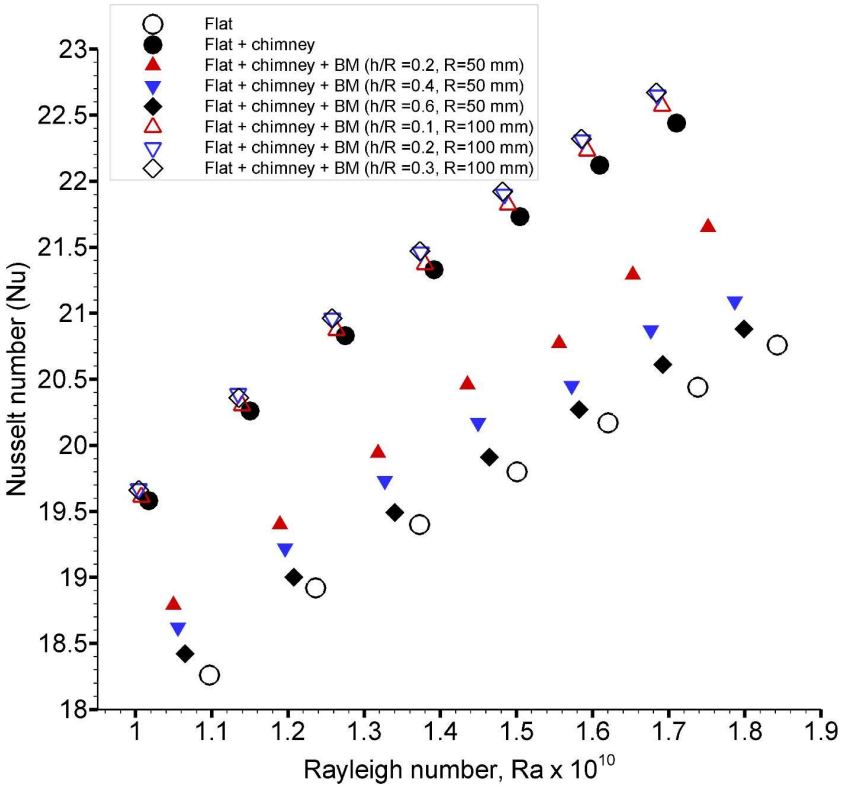

Figure 5.11: Variation of Nusselt number with Rayleigh numbers for various designs (see legend).

contracta increases and hence corresponding pressure decreases. At the vena contracta, the flow cross-sectional area attains minimum value, after which the stream expands again to fill the duct. Note that air enters the inlet at low ambient temperature and gains heat as air travels along the duct. This contraction (of colder air) and expansion (of heated air) creates further vortices which travels downstream. A part of energy that is gained from the absorber plate is lost due to these vortices. Energy losses can be minimized if air entry at the inlet is smooth which is achieved using a bell-shaped design at the inlet (see Fig. 5.12(b)). Using Bernoulli's conservation principle at two sections, the head loss coefficient can be determined in the following form,

$$h_L = \frac{V_2^2}{2g}\left[\left(\frac{A_2}{A_c}\right) - 1\right]^2 = \frac{V_2^2}{2g}\left[\left(\frac{1}{C_c}\right) - 1\right]^2 \tag{5.11}$$

where A_c represents the cross-sectional area of the vena contracta, and C_c is the coefficient of contraction as defined below,

$$C_c = \frac{A_c}{A_2} \tag{5.12}$$

Eq. 5.11 generally expressed using loss coefficient,

$$h_L = K\frac{V_2^2}{2g} \tag{5.13}$$

where, K represents loss coefficient, also expressed as;

$$K = \left[\left(\frac{1}{C_c}\right) - 1\right]^2 \tag{5.14}$$

The values of K is the ratio of the radius of the round corner at the inlet section to the height of the flow channel i.e. (R/H), where R is the radius of round corners and H is the opening of the channel. In fluid dynamic study, the value of K is well documented [27]. However, values of K for the application in solar air

heaters are found wanting. In general, if value of ratio $R/H > 0.2$ then the value of $K = 0.03$, while it is 0.5 for the rectangular shape inlet section (see Fig. 5.12(a)) without round corners [27]. All the designs of bell-mouth considered in the present analysis having values of $R/H > 0.2$, and hence there is a considerable decrease in the entry losses for the case of SAH inlet integrated with bell-mouth design, in comparison to conventional flat rectangular inlet design.

To visualize the effect of bell-shaped inlet in SAH, further simulations are performed for the designs shown in Fig. 5.12(a) and (b). The corresponding flow field are shown in Fig. 5.12(c) and (d) in the form of vorticity. It can be noticed that the SAH with rectangular inlet shows significant spread of vortices inside the duct whereas vorticities are sparsely populated in case of bell-shaped SAH inlet [156, 109]. However, the magnitude of vorticity is higher for bell-shaped design due to higher velocity magnitude. Now the reason behind enhanced mass flow rate in bell-shaped SAH inlet as discussed in the previous sections is clear and it can be attributed to the fact that energy losses are significantly minimized due to the smooth entry of air [156, 109]. Figure 5.12 (e) and (f) shows the corresponding velocity magnitude contour.

5.3.4 Energy conversion efficiency - Which is better: low-temperature high-flow or high- temperature low-flow SAH?

As demonstrated in the previous sections that it is possible to design a solar air heaters that can deliver substantially high mass flow rate with slight reduction in outlet air temperature. This is contrary to what previous researchers have reported i.e. solar energy conversion into heat by increasing the air outlet temperature with a compromise on air mass flow rate. Now the important question arises is: which is better – a slightly low temperature with high flow rate or a high temperature with low flow rate? On the face of it, the later option seems better. We analyzed both the situation from the thermodynamic point of view considering the requirement for space heating application. Similar analogy can be derived for various other applications such as crop drying etc.

Figure 5.13 shows the schematic diagram of a high flow SAH integrated with a $10 \times 10 \times 10$ m space to heat the inside air to a desired temperature of $25°C$. It assumed that no external heat exchange from the control volume (room), no external work done, and flow velocity inside control volume is stagnant.

Mass and energy of the system is conversed at any time. It is given by,

$$\frac{dm_V}{d\tau} = \dot{m}_1 - \dot{m}_2 \tag{5.15}$$

$$\left(\frac{dE}{d\tau}\right)_V = \dot{E}_{in} - \dot{E}_{out} \tag{5.16}$$

where, m_V = mass of fluid in the control volume at any instant, m_1 and m_2 are the mass of the fluid inside the space at their initial and final state, respectively, $\dot{E}_{in}$ and $\dot{E}_{out}$ are the rate of energy enter inside and exit from the control volume. $\dot{E}_{out} = 0$. $\dot{E}_{in}$ is the fluid enthalpy rate at SAH exit which enters the control volume (room) and is equal to $\dot{m}_{in}h_1$.

Considering enthalpy, kinetic and potential energy of the system for an open system, rate of accumulation of energy within the control volume is equal to the net rate of energy flow across the control surfaces and hence,

$$\frac{dE_V}{d\tau} = \left[\left(h_1 + \frac{V_1^2}{2} + Z_1 g\right)\frac{dm_1}{d\tau} + \frac{dQ}{d\tau}\right] - \left[\left(h_2 + \frac{V_2^2}{2} + Z_2 g\right)\frac{dm_2}{d\tau} + \frac{dW}{d\tau}\right] \tag{5.17}$$

where E_V is the energy of fluid enters the control volume at any instant. Other terms have usual meaning. Work done W is zero as there no change in space volume. For the closed system, $V_1 = V_2 = 0$. Since the fluid is air, potential energy gain can be neglected. Here, $h_1 = mC_P T_o$, is the enthalpy of the fluid at the exit of SAH. T_o is air temperature at the outlet of SAH or temperature of air entering the control volume. $P = \rho RT$,$\rho = m/Vol$.

The final form of energy balance equation would be of the form,

$$\dot{m}_{in}h_1 = \frac{d}{d\tau}\left(U_1 - U_2\right) \tag{5.18}$$

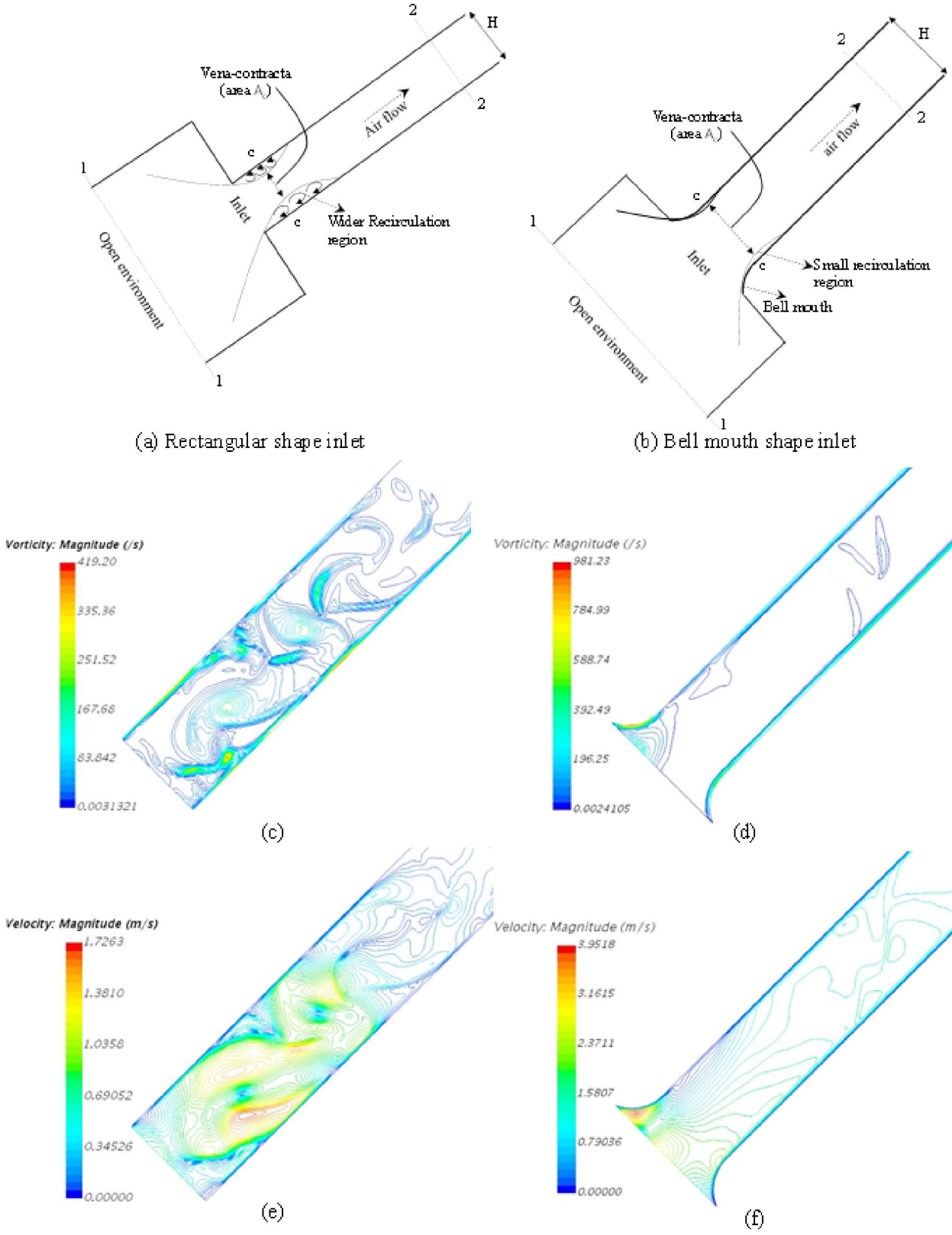

Figure 5.12: Schematic diagram of flow patterns when fluid flows at the inlet of SAH duct with two different inlet designs: (a) Flat rectangular inlet, (b) bell-mouth shape inlet. Notice how the size of vena contracta are different for flat and bell-mouth shape inlet. The vorticity contours when air flows through the SAH duct having: (c) flat rectangular inlet, (d) bell-mouth shape ($h/R = 0.6$, $R = 50\,mm$) inlet. The velocity contours when air flows through the SAH duct having: (e) flat rectangular inlet, (f) bell-mouth shape ($h/R = 0.6$, $R = 50\,mm$) inlet.

where, U_1 and U_2 are the initial and final state internal energy of the fluid in the room. m_1 and m_2 are the mass of the fluid at initial and final state, respectively. Rate of mass change is given by, $\dot{m}_{in} = (m_2 - m_1)/\tau$. The final expression for time duration required to increase the room temperature from initial to final desired state is obtained by integrating the above equation. We get:

$$\tau = \frac{1}{\dot{m}_{in} h_1} \int_1^2 dU \tag{5.19}$$

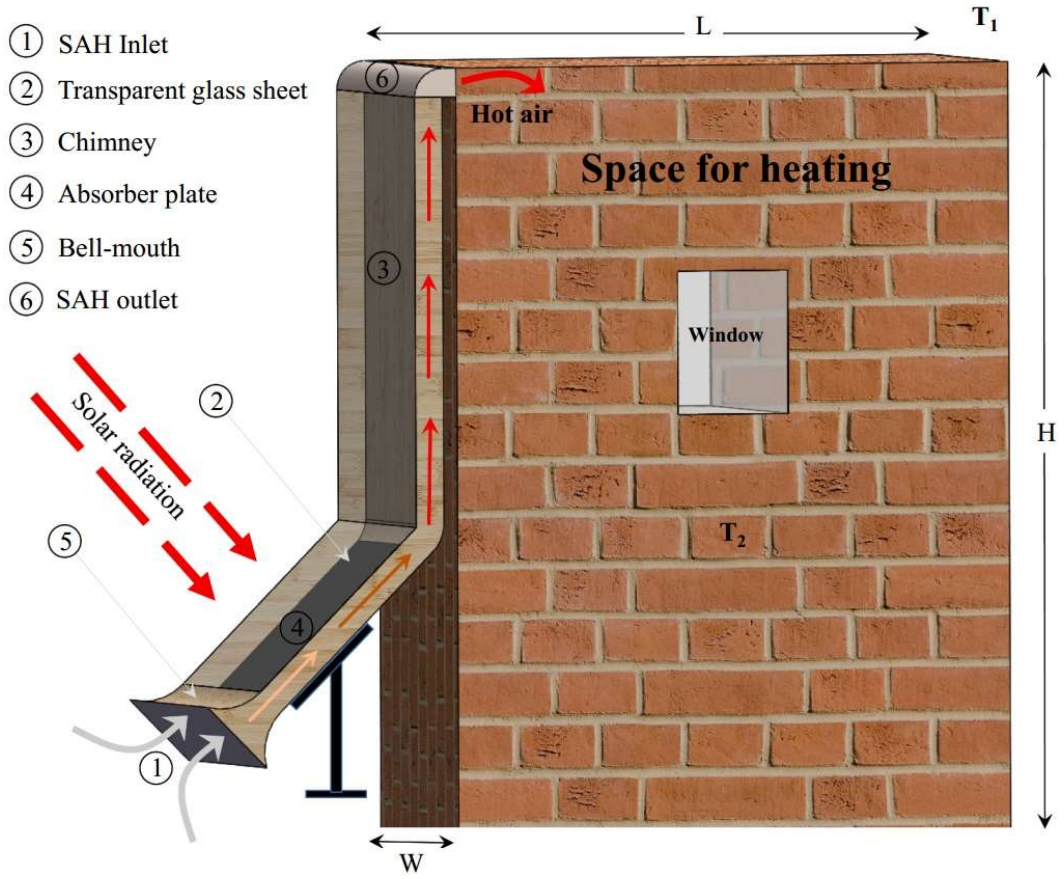

Figure 5.13: High flow SAH integrated with a space having dimensions $L = 10m$, $W = 10m$ and $H = 10m$ for heating in cold climatic condition.

As per above equation, high enthalpy fluid entering the space results in increasing the internal energy of the system. The saving in time achieved over conventional flat plate solar air heaters to reach the same desired temperature of $25°C$ from different initial temperature has been reported in this section. Different ambient temperature T_1 may prevail at different locations across the globe. Following important observations are made:

1. For any value of ambient temperature, conventional SAH performs poorly in terms time required to heat the space to a desired temperature, e.g. when the ambient temperature $T_1 = -5°C$, the conventional SAH takes about 3 hours 30 minutes whereas the combination of bell-mouth with chimney took just about 2 hours 20 minutes. A saving of about 1 hour 10 minutes is substantial. In other words, an improvement of 33% can be considered to be significant while deliberating the intermittent nature of solar radiation during the day time and no sun-shine hours in the night. Clearly, any time saved using SAH during the day is equivalent to increasing the duration of sun-shine hours of that duration. Once the space reaches the final desired temperature, heat losses from the space walls to the ambient would be same for conventional and new designs of SAH. Hence, the high flow SAH would be better suited in maintaining uniform temperature quickly.

2. Another interesting observation is that higher the initial ambient temperature lower would be the time saving with high flow designs of SAH. Clearly, a high flow SAH is better suited for cold climatic conditions.

3. With high flow designs of SAH, additional energy can be saved after the space attains desired temperature. With new energy storage technology such as integrating phase change materials (PCM) in building [68, 34], this additional energy gained can be utilized in increasing the system efficiency further.

The findings of investigations has been shown in Fig. 5.14 displaying the map of design vs. mass flow rate of natural convection SAH. The enhancement in the mass flow rate is higher for the SAH integrated with bell-mouth with chimney effect followed by the combination with bell-mouth alone. Future designs to enhance the SAH mass flow rate could be the use of some innovative materials or designs that incorporate convex or concave type curved SAH [141]. Analysis of proposed new SAH designs can be further investigated using techniques such as artificial neural network and wavelet neural network model [41, 42].

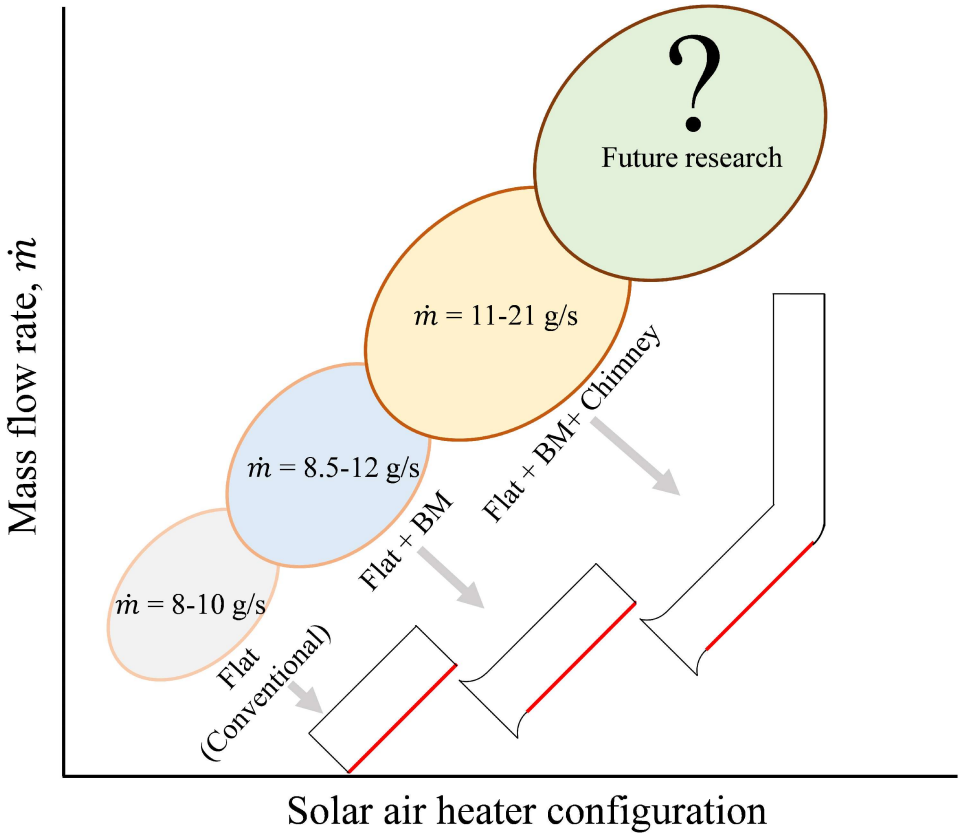

Figure 5.14: Schematic representation of various naturally driven solar air heaters configuration based on their mass flow rates. The mass flow rate values mentioned are for the heat flux 500-1100 W/m^2.

The present investigation would assist in the advancement of natural convection SAH design to make it more suitable for variety of applications where high mass flow rate is the desired outcome.

5.4 Correlation development

In the previous sections, it has been observed that the thermal performance is a strong function of Rayleigh numbers (Ra) and ratio 'h/R' for the design of SAH with bell-mouth while operating on natural convection principle. An individual correlation for SAH with different designs of bell-mouth has been developed. 21 data points per variables are used for correlations development though minimum 10 data points per variable is considers appropriate. The functional relationship of Nusselt number with the influencing parameters may be written as:

$$Nu = f\left(Ra\, cos\theta, h/R\right) \tag{5.20}$$

The relationship between the Nusselt number and Rayleigh number results in power law in the form given below:

$$Nu = A_o \ (Ra\, cos\theta)^m \, (h/R)^n \tag{5.21}$$

In order to obtain the relationship between Nusselt number and Rayleigh number, variation of $ln\,(Nu)$ versus $ln(\ Ra\, cos\theta\ \ )$ for different values of 'h/R' have been shown in Fig. 5.15. The relationship between $ln\,(Nu)$ versus $ln\,(Ra\, cos\theta)$ is observed to vary according to a power law. Hence, logarithmic form of equation can be written as:

$$ln\ (Nu) = A_o \ [ln\,(Ra\ cos\theta)]^m \tag{5.22}$$

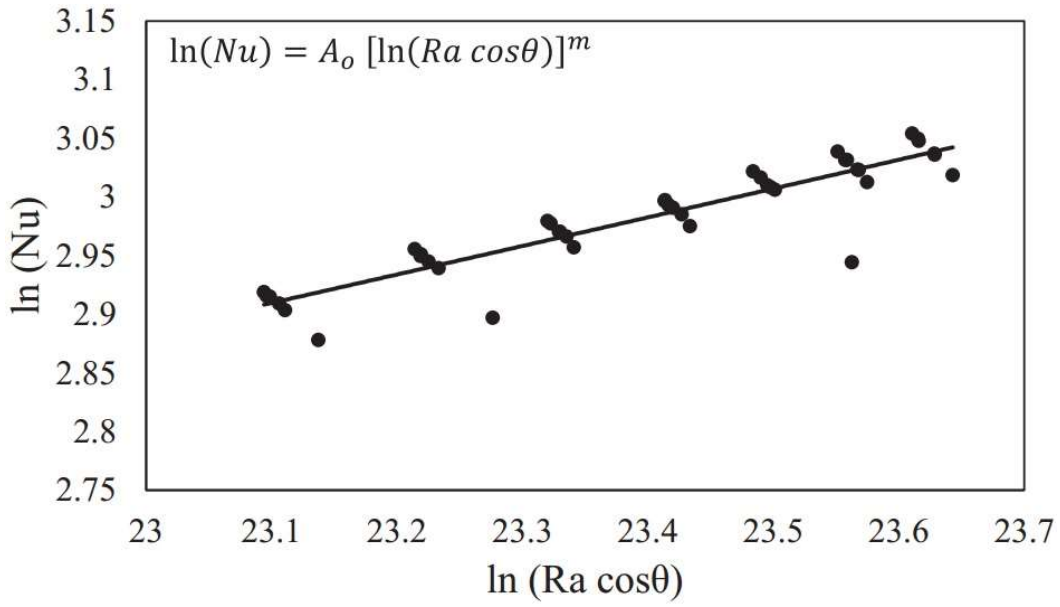

Figure 5.15: Plot of $ln\,(Nu)$ versus $ln\,(Ra\, cos\theta)$ of flat natural convection SAH having bell-mouth shape inlet.

Above relation has been obtained using relevant data points fitted with R-square method as shown in Fig. 5.15.

To get the power law relation between $ln\,(A_o)$with $ln\,(h/R)$, the trend observed in the plot using all the data point is given as;

$$ln\ (A_o) = B_o \ [ln\,(h/R)]^n \tag{5.23}$$

where coefficient $B_o = \frac{ln(Nu)}{[ln(Ra\, cos\theta)]^m [ln(h/R)]^n}$ is a function of Nu, Ra andϕ.

The final correlation after rearranging Eq. 5.22 and 5.23 has been obtained for Nusselt number is shown below;

$$ln\,(Nu) = C_o\,[ln\,(Ra\, cos\theta)]^m \ \left[ln\left(\frac{h}{R}\right)\right]^n \tag{5.24}$$

where $C_o = 0.0089$, $m = 1.9186$, and $n = -0.007$. Note that the correlation has been obtained for $\theta = 45°$, which is constant in our study.

The correlation developed for Nusselt number (refer Eq. 5.24) for different designs of bell-shaped inlet of natural convection SAH. Figure 5.16 shows the variation of Nusselt number obtained using correlation with respect to numerical data. The mean percentage deviation of Nusselt number obtained by correlation is found to be 2.1%, which comes under acceptable limits and shows excellent agreement with the CFD values. The correlation can be used to determine the Nusselt number with reasonable accuracy.

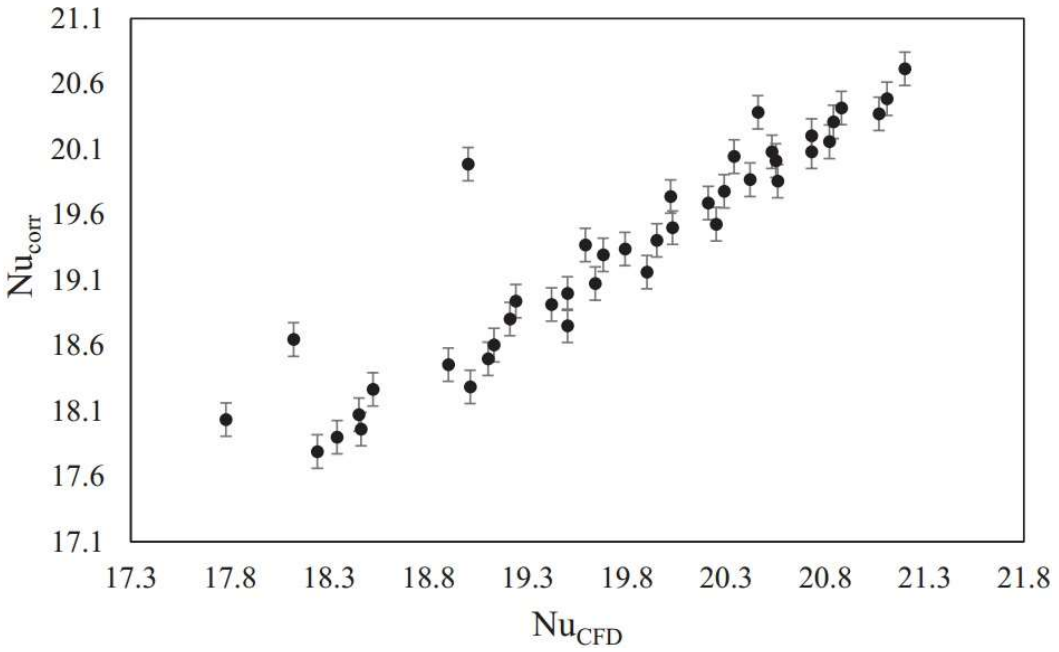

Figure 5.16: Comparison between values of Nu_{corr} and Nu_{CFD} of flat natural convection SAH having bell-mouth shape inlet.

5.5 Conclusion

Low adoption of natural convection solar air heaters for wide applications has been mostly due to its low air mass flow rates. In this chapter, investigations have been performed for new designs of SAH with an aim to increase the mass flow rates without considerably altering the basic design of SAH. Integration of various designs of bell-shaped inlet and chimney at the outlet with the conventional SAH shows considerable enhancement in thermo-hydraulic performance. The range of parametric ratio h/R of bell-mouth design investigated was $0.1 \leq h/R \leq 0.6$ for solar insolation range $500 - 1100$ W/m^2. Following major conclusions are drawn from the study:

1. Integration of bell-mouth at the inlet of conventional naturally driven flat SAH always increases the mass flow rates of heated air.

2. The thermo-hydraulic performance is significantly enhanced by increasing h/R ratio when integrated with chimney. Higher h/R ratio indicates large inlet opening. Higher h/R ratio gives better thermo-hydraulic performance at higher solar insolation.

3. Due to enhance mass flow rate, significant drop in pressure coefficient of about 22% was observed with bell-mouth and chimney in comparison to conventional flat SAH.

4. In the range of parameters investigated, the highest mass flow rate of 111% was observed for bell-mouth design of $h/R = 0.3,\ R = 100mm$ when integrated with chimney.

5. Integration of bell-shaped inlet minimizes the entry losses by reducing the formation of recirculating vortices in the SAH duct and, thereby resulting in significant drop in hydraulic losses and hence, enhances the mass flow rate.

6. The pertinent question on energy conversion efficiency of SAH that has not been investigated before is: which is better – a low-flow high-temperature system or high-flow low-temperature system. In this chapter, we have shown that when the SAH is integrated with application such as space heating, the later system with high-flow low-temperature shows better solar energy conversion with significant saving in sun-shine hours. It was also observed that a high-flow low-temperature solar air system is better suited for cold climatic conditions where ambient temperature is low.

7. An independent correlation for Nusselt number variation as a function of Rayleigh numbers and bell-mouth ratio h/R. It varies as $ln\,Nu \sim [ln\,(Racos\theta)]^m \left[\ln\left(\frac{h}{R}\right)\right]^n$ where m and n are constants. The relation showed excellent agreement with the numerical results with mean percentage deviation of 2.1% with respect to numerical data.

The authors hope that data and design presented in this research would give a new direction for efficient designs of naturally driven solar air heaters that can cater to the needs of various applications needing higher mass flow rates. Future research may focus on investigating the effect of various chimney designs and its integration with bell shaped inlet with convex or concave type curved SAH [141].